


RESEARCH ARTICLE | MARCH 06 2018

# Towards terahertz detection and calibration through spontaneous parametric down-conversion in the terahertz idler-frequency range generated by a 795 nm diode laser system

Special Collection: [Frontiers in THz Photonic Devices](#)

Vladimir V. Kornienko ; Galiya Kh. Kitaeva; Florian Sedlmeir; Gerd Leuchs ; Harald G. L. Schwefel 

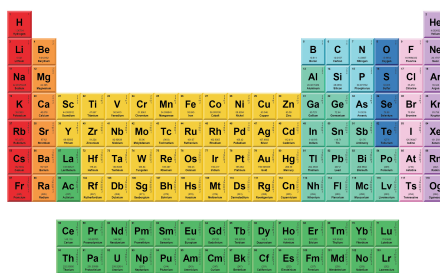


APL Photonics 3, 051704 (2018)  
<https://doi.org/10.1063/1.5011201>



THE MATERIALS SCIENCE MANUFACTURER®

**Now Invent.™**



American Elements  
 Opens a World of Possibilities

...Now Invent!

[www.americanelements.com](http://www.americanelements.com)

© 2017-2024 American Elements is a U.S. Registered Trademark



# Towards terahertz detection and calibration through spontaneous parametric down-conversion in the terahertz idler-frequency range generated by a 795 nm diode laser system

Vladimir V. Kornienko,<sup>1,2,a</sup> Galiya Kh. Kitaeva,<sup>2</sup> Florian Sedlmeir,<sup>3,b</sup> Gerd Leuchs,<sup>3,4</sup> and Harald G. L. Schwefel<sup>5,c</sup>

<sup>1</sup>All-Russia Research Institute of Automatics (VNIIA), 22 Sushchevskaya Str., Moscow 127055, Russia

<sup>2</sup>Faculty of Physics, M. V. Lomonosov Moscow State University, 1-2 Leninskie Gory Str., GSP-1, Moscow 119991, Russia

<sup>3</sup>Max Planck Institute for the Science of Light, 2 Staudtstrasse, Erlangen 91058, Germany

<sup>4</sup>University of Erlangen-Nürnberg, 7/B2 Staudtstrasse, Erlangen 91058, Germany

<sup>5</sup>The Dodd-Walls Centre for Photonic and Quantum Technologies, Department of Physics, University of Otago, Dunedin, New Zealand

(Received 30 October 2017; accepted 13 February 2018; published online 6 March 2018)

We study a calibration scheme for terahertz wave nonlinear-optical detectors based on spontaneous parametric down-conversion. Contrary to the usual low wavelength pump in the green, we report here on the observation of spontaneous parametric down-conversion originating from an in-growth poled lithium niobate crystal pumped with a continuous wave 50 mW, 795 nm diode laser system, phase-matched to a terahertz frequency idler wave. Such a system is more compact and allows for longer poling periods as well as lower losses in the crystal. Filtering the pump radiation by a rubidium-87 vapor cell allowed the frequency-angular spectra to be obtained down to  $\sim 0.5$  THz or  $\sim 1$  nm shift from the pump radiation line. The presence of an amplified spontaneous emission “pedestal” in the diode laser radiation spectrum significantly hampers the observation of spontaneous parametric down-conversion spectra, in contrast to conventional narrowband gas lasers. Benefits of switching to longer pump wavelengths are pointed out, such as collinear optical-terahertz phase-matching in bulk crystals. © 2018 Author(s). All article content, except where otherwise noted, is licensed under a Creative Commons Attribution (CC BY) license (<http://creativecommons.org/licenses/by/4.0/>). <https://doi.org/10.1063/1.5011201>

## I. INTRODUCTION

One of the most mysterious processes in nonlinear optics is that of spontaneous parametric down-conversion (SPDC). Quantum mechanical zero-vacuum fluctuations induce the spontaneous decay of a pump photon (at frequency  $\omega_p$ ) into two lower energy photons, namely, signal ( $\omega_s \geq \omega_p/2$ ) and idler ( $\omega_i \leq \omega_p/2$ ) photons.<sup>1</sup> Without quantum mechanics, such decay can only be stimulated by the presence of additional photons (either signal or idler) within the nonlinear medium. This is particularly the case when a nonlinear optical detector is fed at the idler wave frequency with an external radiation to be measured. Strict correlation of frequencies and wavevectors between signal and idler waves can be used to detect the spectrum of external radiation at idler frequency  $\omega_i$  by measuring the up-converted optical signal wave ( $\omega_s$ ) generated in the nonlinear interaction. This interplay between the classical and quantum processes forms the basis of the quantum brightness calibration scheme (see Refs. 2–8

<sup>a</sup>E-mail: [vv.kornienko@physics.msu.ru](mailto:vv.kornienko@physics.msu.ru)

<sup>b</sup>[florian.sedlmeir@mpl.mpg.de](mailto:florian.sedlmeir@mpl.mpg.de)

<sup>c</sup>[harald.schwefel@otago.ac.nz](mailto:harald.schwefel@otago.ac.nz)

for original studies and Refs. 9 and 10 for the terahertz frequency range), whereby the spectral brightness of a given external terahertz-wave (THz) source can be directly determined in absolute units (Watts). This is of particular value in the THz range due to the deficiency of calibrated sources and detectors. Registration of the frequency-angular SPDC spectra is at the basis of the idler wave spectral brightness calibration procedure. A brief review of metrology applications of the method can be found in Sec. 5.4.2 of Ref. 6.

In this paper, we use the SPDC spectroscopy as a tool for indirect evaluation of terahertz-wave detector spectral sensitivity. Only the signal wave is detected, and the corresponding properties of a terahertz wave (frequency and wavevector) are calculated using the (quasi-)phase-matching conditions. A prime advantage of this method is that no THz source is needed when evaluating the spectral sensitivity of a detector. These measurements are furthermore ideally suited to study the properties of nonlinear crystals in the THz range,<sup>11,12</sup> in particular, the crystals with spatial modulation of their nonlinear susceptibility.<sup>11–17</sup>

The main applied challenge in SPDC spectroscopy in the THz range of idler frequencies is the need to detect extremely small signals spectrally close to a strong optical pump, which are shifted by only about  $5\text{--}100\text{ cm}^{-1}$  (0.2–3 THz). Up to now, this has only been achieved by utilizing a gas laser radiation source, where introducing a Fabry–Pérot etalon into the laser cavity further narrows the lasing wavelength. After passing through the nonlinear crystal, the pump radiation is filtered by a narrowband frequency filter, most commonly a gas absorption cell.<sup>9,18–20</sup>

Here we propose and experimentally study a different approach based on the use of a near infrared diode laser system. Diode lasers are known to be more reliable, compact, and convenient pump radiation sources as compared to gas lasers. Also, our system provides a longer pump wavelength which allows one to: employ larger periods of spatial modulation in periodically poled structures, operate at lower THz frequencies where the crystal is less absorptive, fulfill the phase-matching conditions for the backward-propagating THz waves in a bulk crystal, and simultaneously observe several orders of quasi-phase-matching in a single crystal, as discussed below.

The main drawback of a diode laser is the broad bandwidth of their gain and the resulting amplified spontaneous emission (ASE) background due to the sub-threshold amplification of spontaneous emission. ASE typically covers all the gain bandwidth spectral range and significantly hampers the registration of SPDC spectra and inhibits the possibility of increasing the signal-to-noise performance of a setup via increasing the exposure times. By carefully filtering the ASE, we report here our results on observing the spontaneous parametric conversion spectra in the THz range of idler wave frequencies, using a commercial 795 nm pump diode laser system. Numerical and experimental results are provided for differently poled lithium niobate (LiNbO<sub>3</sub>) crystals.

## II. PHASE MATCHING FOR PARAMETRIC FREQUENCY CONVERSION

In a parametric frequency converter based on a  $\chi^{(2)} \neq 0$  medium, two processes can occur leading to the creation of signal ( $\omega_s$ ) photons. First, it is the decay of a pump photon ( $\omega_p$ ) into a lower frequency ( $\omega_{St} = \omega_p - \omega_i$ ) “Stokes” signal photon together with the emission of an additional idler photon ( $\omega_i$ ). In the case of spontaneous decay (no external radiation), this process is referred to as the SPDC, and in the case of external-radiation-induced conversion, it is called difference frequency generation. Second, it is the combination of a pump and a noise photon, or an external one, into a higher frequency “anti-Stokes” ( $\omega_{AS} = \omega_p + \omega_i$ ) signal photon, the so-called spontaneous parametric up-conversion (SPUC), or sum frequency generation, correspondingly. To be short, we shall refer to these two processes as a “Stokes interaction” and an “anti-Stokes interaction.” In the optical range, thermally induced noise photons are negligible and the contribution from the zero-vacuum fluctuations (i.e., the spontaneous decay acts) are dominant, while in the radio frequency range thermal noise (Planck black body radiation) prevails. In the terahertz (THz) frequency domain (and at room temperature), spectral densities of both contributions are of the same order of magnitude. We shall henceforth denote all the effects taking place under the optical pumping but without an external THz-wave source as “spontaneous parametric conversion” (SPC) encompassing both SPDC and SPUC. By comparing

the optical Stokes and anti-Stokes photons, sensitivity can be significantly improved<sup>2,3,9,11,12,20</sup> of a nonlinear optical detector of THz radiation.

Energy conservation law results in a strict condition on the frequencies of interacting waves,  $\omega_p = \omega_s \pm \omega_i$ . This is however not the only requirement, as parametric frequency conversion is most efficient when momentum conservation (i.e., the phase-matching condition) is met. These conditions are fulfilled if the wavenumber mismatch between the interacting waves vanishes [see also Figs. 1(a), 1(c), and 1(d)],  $\Delta\vec{k} \equiv \vec{k}_p - (\vec{k}_s + \vec{k}_i) = 0$  for the Stokes interaction and  $\Delta\vec{k} \equiv \vec{k}_s - (\vec{k}_p + \vec{k}_i) = 0$  for the anti-Stokes interaction. With both energy and momentum conservation in place, SPC optical signal  $\omega$ - $\mathbf{k}$  frequency-angular distribution reproduces<sup>1,9,20</sup> the  $\omega$ - $\mathbf{k}$  sensitivity of a nonlinear-optical spectrally resolved THz-wave detector. If an SPC spectrum for a signal wave is observed, the well detectable power of THz radiation by the same nonlinear detector can be estimated as  $N_{\text{THz}} \sim (1 + (\exp(\hbar\omega_{\text{THz}}/k_B T) - 1)^{-1}) \sim 7$  photons per radiation mode at 1 THz at room temperatures, provided the uniform filling of the input modes of parametric frequency converter with external THz radiation.

A spatially non-uniform distribution of the nonlinear susceptibility allows for quasi-phase matching (QPM) which provides additional tuning of the phase-matched frequencies.<sup>13–17</sup> In the case of SPDC in periodically poled crystals, it has the following form:

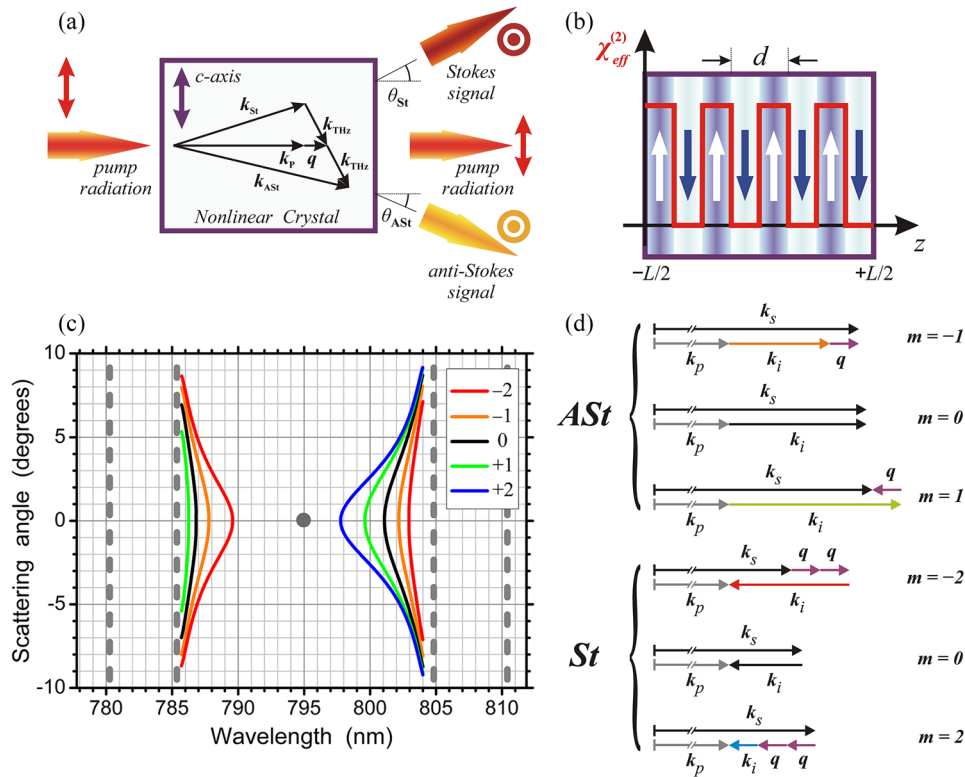


FIG. 1. (a) (side view) The first order ( $l=1$ ) type-I (“*ooe*”) quasi-phase-matching (QPM) in a (b) periodically poled lithium niobate crystal (PPLN) with a given poling period  $d$  and an optical axis (“*c*-axis”) shown with white and blue arrows. For a given terahertz wave propagation direction, the corresponding Stokes and anti-Stokes signals have opposite signs of the angle  $\theta$ . Polarizations of the interacting waves are shown in (a) with double-sided arrows (“vertical,” extraordinary) and concentric circumferences (“horizontal,” ordinary). (c) Frequency-angular QPM tuning curves for a PPLN with  $|q| = 2\pi/33 \mu\text{m}$  under 795 nm pumping, calculated for QPM orders  $m = -2$  to  $+2$  as specified in the inset. At every point of the colored curves, the phase mismatch is exactly zero. The gray circle shows the pump radiation wavelength. Dashed gray lines denote *E*-type transverse-optical phonons in lithium niobate:  $152.8 \text{ cm}^{-1}$  (4.6 THz) and  $238.3 \text{ cm}^{-1}$  (7.2 THz). Terahertz-range dispersion properties are taken from Refs. 21–23. (d) Wavevector diagrams for quasi-phase-matched collinear interaction for the QPM curves from (c). “St” stands for the Stokes interaction ( $\omega_p = \omega_s + \omega_i$ ), “ASt” stands for the anti-Stokes one ( $\omega_p = \omega_s - \omega_i$ ). “(THz-)Backward” geometry takes place for the Stokes range interaction. Pump and signal wavevectors’ lengths are not to scale.

$$\Delta \vec{k} \equiv (\vec{k}_p + m\vec{q}) - (\vec{k}_s + \vec{k}_i) = 0. \quad (1)$$

Here,  $\vec{q}$  ( $q = 2\pi/d$ ) is a reciprocal super-lattice wavevector that characterizes the nonlinear medium,  $d$  is a nonlinear susceptibility modulation period, and  $m = 0, \pm 1, \pm 2, \dots$  is an integer and is referred to as the order of quasi-phase-matching or the QPM order. Equation (1) can be simplified by taking into account the significant difference in frequency ( $\omega_p/\omega_i \sim 10^3$ ) between optical and THz waves. In the case of the collinear interaction, Eq. (1) can be rewritten as follows:

$$\Delta k_{\parallel} \equiv \frac{\omega_i}{u_{gr}^{opt}} \mp \frac{\omega_i n_i}{c} + m q_{\parallel} + \Delta k_0 = 0. \quad (2)$$

Here,  $c/n_i$  is the phase velocity of the THz idler wave,  $u_{gr}^{opt} \equiv \frac{\partial \omega}{\partial k} \Big|_{\omega \approx \omega_p}$  is the group velocity of the optical wave around the pump frequency,  $q_{\parallel}$  is the projection of  $\vec{q}$  on the pump radiation propagation direction, and the constant  $\Delta k_0 \equiv k_p(\omega_p) - k_s(\omega_p)$  allows for different polarizations of pump and signal waves in a birefringent material. The plus sign in Eq. (2) denotes the case of counter-propagating THz and pump waves (“backward geometry”), the minus sign denotes that of co-propagating (“forward geometry”) waves [Fig. 1(d)]. For any given modulation period  $d$  and QPM order  $m$ , the propagation direction of the terahertz idler wave associated with the collinear Stokes and anti-Stokes interactions are opposite [Figs. 1(d) and 2].

Switching from the traditionally used  $\lambda_p = 514.5$  nm pump wavelength (argon ion laser)<sup>9,11,19</sup> to  $\lambda_p = 795$  nm (diode laser) has several advantages. First, the frequencies of the quasi-phase-matched THz waves are decreased (for a given modulation period  $d > 10 \mu\text{m}$ ) (Fig. 2). This increases the usability as the THz detector, as for higher THz frequencies the absorption within the lithium niobate crystal grows drastically ( $\sim 100 \text{ cm}^{-1}$  and greater) as the phonon resonance (around 7.4 THz) is approached. Furthermore, one can employ longer periods which facilitate the fabrication of periodically poled crystals. Second, it becomes possible to simultaneously fulfill the QPM conditions in a single crystal at a set of frequencies [see Fig. 2(b)], which can be exploited in multi-frequency spectroscopy tasks. Quasi-phase-matched crystals for THz wave detection benefit from frequency-selective response tuned with structural (rather than material) properties, and from enabling a collinear interaction at the desired THz frequency, as illustrated in Figs. 1(c) and 2. Third, the “backward”-type collinear phase-matched optical-terahertz interaction for  $m = 0$  (i.e., the case of a bulk crystal) becomes possible [see Fig. 4 and black curves in Fig. 1(c)] due to the particular dispersion properties of lithium niobate. This interaction is only possible due to the significant difference between the wavevector values of optical ( $\sim 10^1 \mu\text{m}^{-1}$ ) and terahertz ( $\sim 10^{-1} \mu\text{m}^{-1}$ ) waves. In the optical range, conversion processes in “backward” geometry are only feasible within very small coherent buildup lengths or in multiple-domain crystals with extremely small ( $\sim 0.1 \mu\text{m}$ ) thickness of oppositely polarized layers. Bulk crystals are superior over the periodically poled crystals in terms of fabrication challenges and repeatability issues.

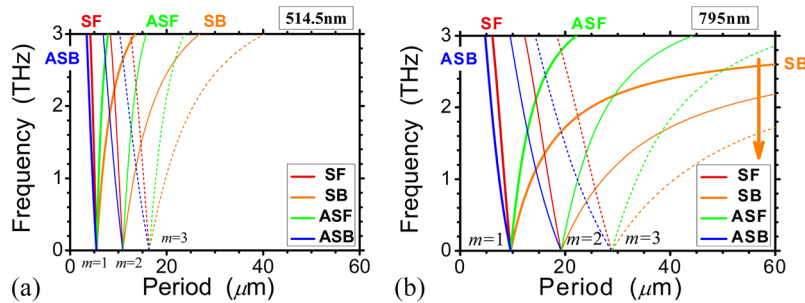


FIG. 2. Collinear quasi-phase-matching (QPM) tuning curves for different QPM orders ( $m = -3$  to  $+3$ ) in a lithium niobate crystal under (a) 514.5 nm and (b) 795 nm pumping. Calculations are presented for Stokes (“S”) and anti-Stokes (“AS”) interaction types in “(THz-)forward” (“F”) and “(THz-)backward” (“B”) propagating geometries. Simultaneous observation of a few QPM tuning curves (SB,  $m = 1, 2, 3$ ) in a single crystal ( $d \sim 57 \mu\text{m}$ ) is shown in (b) with an orange arrow. Terahertz-range dispersion properties were taken from Refs. 21–23.

### III. EXPERIMENTAL SETUP

For the experimental setup, depicted in Fig. 3(a), we used an external cavity stabilized diode pump laser with the central wavelength around 795 nm giving up to 50 mW of continuous wave optical power (TOPTICA DL100). For the amplified spontaneous emission suppression, we used a pair of extremely narrowband frequency filters (HWHM  $\sim 5 \text{ cm}^{-1}$  or  $\sim 0.3 \text{ nm}$  at 795 nm central wavelength; contrast  $\geq 20 \text{ dB}$ ) based on reflection-type holographic diffraction gratings (Ondax NoiseBlock). Two consecutive polarizing beam splitters cleaned up the polarization of the laser and then illuminated the nonlinear medium. We used lithium niobate crystals (Mg:Y: LiNbO<sub>3</sub>) with an in-growth domain structure, grown by the Czochralski method in an asymmetric thermal field from a congruent melt, doped with magnesium (Mg 2 mol. %) and yttrium (Y 0.5 mol. %).<sup>24–27</sup> Choosing an optimal crystal growth direction allows one to create “facet”-type crystals with superior parameters (domain wall thickness, large size, homogeneity).<sup>28</sup> Magnesium (Mg) doping lowers the absorption at terahertz frequencies by reducing the number of crystal structure defects.<sup>21</sup> The use of “QPM crystals” instead of bulk ones was motivated by the presentation purposes only, for it yields QPM at lower terahertz frequencies and more branches of QPM [see Fig. 1(c)]. There are two most common (quasi-)phase-matching geometries for lithium niobate at terahertz frequencies: “*eee*” (“type-0”)—all the waves are extraordinary polarized, with the highest nonlinear susceptibility component value available,  $\chi^{(2)}_{zzz} \equiv 2d_{33} \sim 50 \text{ pm/V}$ —and “*ooe*” (“type-I”)—an extraordinary pump wave and ordinary signal and idler waves, with  $\chi^{(2)}_{xxz} \equiv 2d_{15} \sim 5 \text{ pm/V}$ .<sup>29</sup> For noise suppression, we used the “*ooe*” interaction [see Figs. 1(a) and 3(a) for polarizations of the interacting waves], albeit at the cost of reducing the effective nonlinear coefficient value. Namely, an additional attenuation of the pump and ASE radiation after the crystal at the level of  $\sim 10^3$  has been achieved with crossed polarizers, and the SPDC power ( $P \sim (\chi^{(2)}_{ijk})^2$ ) has been lowered by a factor of  $\sim 100$ . The residual pump radiation was subsequently blocked via a narrowband gas filter (Precision Glassblowing, USA). We used the  $D_1$  ( $5^2S_{1/2} \rightarrow 5^2P_{1/2}$ ,  $\sim 795 \text{ nm}$ ) transition of rubidium-87 (<sup>87</sup>Rb) for this purpose. Finally, a monochromator (Zolix) provided the spectral separation, and the frequency-angular signal radiation spectrum was detected with a CCD camera (Andor iKon-M 934). The dynamic range of the CCD camera was  $6 \times 10^4$  counts, and the lowest detectable power of an optical signal was  $\sim 10^{-17} \text{ W}$  ( $\sim 100$  counts at 100 s exposure value) limited by an interplay between a CCD readout noise and a charge spread due to the residual pump radiation. The frequency and wavenumber of an idler wave

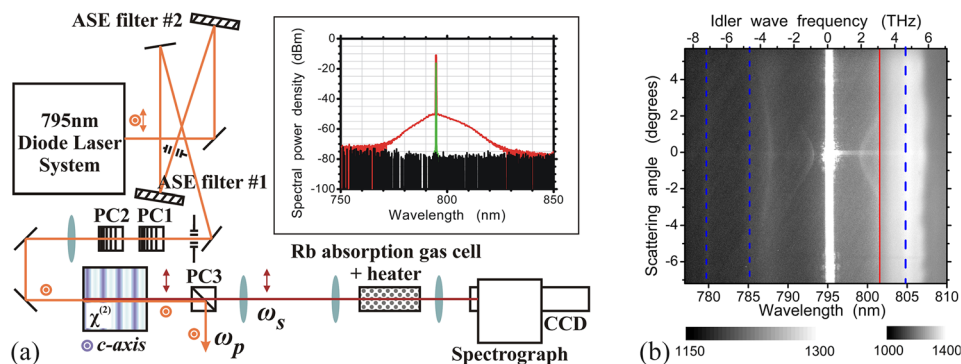


FIG. 3. (a) (Top view) Experimental setup for frequency-angular spontaneous parametric conversion (SPC) spectra observation. “PC”—polarizing prisms for polarization control. Light polarization as well as the nonlinear crystal axis (“*c-axis*”) is depicted by double-sided arrows (“horizontal,” ordinary) and concentric circumferences (“vertical,” extraordinary). The inset shows the wavelength spectrum (in dBm) of the diode laser system (red curve, broadband ASE “pedestal”) and that of the radiation reflected from the first ASE filter (narrow green curve). The detector noise floor is shown in black. (b) Frequency-angular SPC spectra in a periodically poled lithium niobate (Mg:LiNbO<sub>3</sub>) crystal. The domain structure period is  $\sim 20 \mu\text{m}$ ; the exposure time is 10 s. Terahertz-wave frequencies in the anti-Stokes range are marked with a minus sign. Dashed blue curves denote near-forward Raman signal due to *E*-type transverse-optical phonons:  $152.8 \text{ cm}^{-1}$  (4.6 THz) and  $238.3 \text{ cm}^{-1}$  (7.2 THz). The grayscale color shows the signal intensity in the linear scale. Different grayscales are used in regions separated with a solid line for the presentation purposes due to the low power of the SPDC signal.

corresponding to the detected signal can easily be calculated using the phase-matching conditions from Eqs. (1) and (2). Similar setups are described in Refs. 9, 10, 19, and 20.

#### IV. RESULTS AND DISCUSSION

A typical experimental SPC frequency-angular spectrum observed with a CCD camera is presented in Fig. 3(b). A bright vertical line at the centre of the image corresponds to the pump radiation wavelength (795 nm) and is the result of elastic scattering of pump radiation in the elements of the experimental setup, including the gas filter. The horizontal line in the image centre is the trace of the residual ASE radiation transmitted through the spectral filtering system and eventually shows the line of zero scattering angles (collinear interaction). Bright vertical lines both in Stokes [to the right from the pump radiation line in Fig. 3(b)] and anti-Stokes (to the left) ranges, marked with blue dotted lines, originate from the Raman scattering of the pump radiation due to *E*-type transverse optical phonons in lithium niobate<sup>30</sup> located at  $152.8\text{ cm}^{-1}$  (4.6 THz) and  $238.3\text{ cm}^{-1}$  (7.2 THz), respectively. When the dynamical range of a CCD camera is exceeded, charges can spread over adjacent photosensitive elements (pixels), limiting the maximum exposure time value. It is prominently visible as the thick bright vertical line at  $\sim 795\text{ nm}$  [Fig. 3(b)] due to the residual pump radiation, with the thickness increasing with the exposure time (not shown in the Figure). Thus, even the most narrowband signal such as the residual background ASE radiation not being filtered out by the diffraction filters resulted in substantial noise in the CCD-camera readings. Curved lines correspond to our main result, the SPC signal radiation. Both processes—the spontaneous quantum zero-vacuum fluctuation-stimulated signals and the thermal THz photon-induced signals—are observable. The obtained results allow us to conclude that in the case of pump laser systems with a wide gain bandwidth, a thorough spectral filtering of their ASE radiation is required. One of the promising approaches for the future may be the (intra-cavity) frequency doubling of the pump laser radiation. This method allows one to obtain a narrow-band radiation without the spectral ASE “pedestal” due to the quadratic scaling of second harmonic generation with the pump power. Another option is to exploit a combination of interference-type spectral devices, such as Fabry–Pérot etalons with different finesse, and diffraction gratings or narrowband filters based on optical whispering gallery modes.<sup>31</sup> However, these approaches lead to a significant complication of the experimental setup.

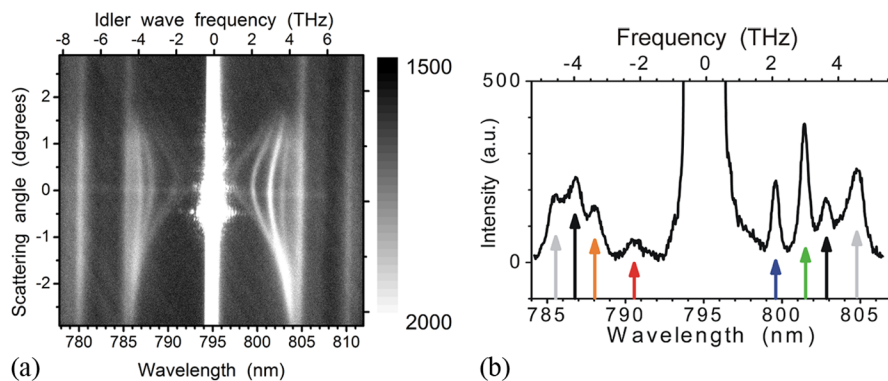


FIG. 4. Simultaneous observation of several quasi-phase-matching (QPM) orders in a lithium niobate single crystal with aperiodical domain structure. See Fig. 1(c) for the numerical results and Fig. 1(d) for the wavevector diagrams. Terahertz-wave frequencies in the anti-Stokes range are marked with a minus sign. Bulk interaction ( $m = 0$ ) takes place for backward terahertz waves in the Stokes region. Image distortions in (a), such as the overall tilt and the mismatch in the zero angle positions for tuning curves of different QPM orders, are due to misalignments in the experimental setup, such as displacement of the optical axis of the system relative to the monochromator slit position, introduced in order to improve the suppression of the transmitted pump radiation. The grayscale shows the intensity in the linear scale. (b) The central region of the zero scattering angle cross section of (a) (i.e., the collinear interaction). Gray arrows denote Raman peaks from the *E*-type  $152.8\text{ cm}^{-1}$  phonon. QPM orders are shown with color arrows [see also Fig. 1(d) with the same color legend for terahertz waves]: (left to right)  $m = 0$ ,  $m = -1$ , and  $m = -2$  (anti-Stokes region) and  $m = +2$ ,  $m = +1$ , and  $m = 0$  (Stokes region).

In the case of crystals with non-regular spatial  $\chi^{(2)}(\mathbf{r})$  distribution, it is possible to simultaneously observe quasi-phase-matched processes occurring at different frequencies of signal and idler waves. Figure 4(a) shows the experimental SPC frequency-angular spectrum with a few “branches” of parametric scattering in different QPM orders  $m$ . The “Horizontal” (zero angle) cross section of Fig. 4(a) is given in Fig. 4(b) along with the QPM order designation (color arrows), while the wavevector diagrams are available in Fig. 1(d). The calculated scattering angles corresponding to the exact (quasi-)phase-matching for different QPM orders ( $m = -2, \dots, +2$ ) for this crystal are shown in Fig. 1(c). Calculation was based on the results of measuring the crystal period via the SPC characterization method under 514.5 nm pumping, with the dispersion properties taken from Refs. 21–23. Bulk interaction ( $m = 0$ ) takes place for backward terahertz waves in the Stokes region.

## V. SUMMARY

We have experimentally measured and theoretically predicted the spontaneous parametric up- and down-conversion spectra under 50 mW 795 nm diode laser system pumping, in the THz range of idler wave frequencies. The most critical experimental challenge was the broad ASE spectrum of the diode laser. The central pump radiation was filtered through a rubidium-87 ( $^{87}\text{Rb}$ ) vapor cell, but the presence of broad ASE spectrum significantly hampered the observation of the SPC spectra, in contrast to conventional narrowband gas lasers. The particular narrowband frequency filters used were based on holographic diffraction gratings that are not optimal for spectral filtering due to the mismatch in bandwidth between them and the gas filter that leads to intolerably high residual radiation power near the laser line frequency.

Considering the nonlinear crystal as a detector of THz waves, adjusting the pump radiation frequency can change the acceptance range of the THz idler wave. We have demonstrated the possibility of phase-matched collinear interaction between optical waves and a “backward”-propagating terahertz wave. Furthermore, we showed that simultaneous observation of quasi-phase-matching in different orders is possible which will allow for large bandwidths in THz detection schemes. The experimental results were demonstrated for a lithium niobate crystal with a spatially heterogeneous distribution of the second-order nonlinear susceptibility, but the method is also valid for bulk crystals. Increasing the pump wavelength allows one to employ bulk crystals for collinear phase-matched optical-terahertz interaction and also to use periodically poled crystals with greater modulation periods.

Further advances of the proposed technique are associated with narrowing the linewidth of the pump radiation source. The following approaches may be surmised: (1) frequency-doubling for ASE background suppression and (2) frequency filtering by means of several high-Q interference devices such as Fabry–Pérot etalons and others, along with more elaborate polarization filtering.

## ACKNOWLEDGMENTS

We acknowledge financial support from the Russian Science Foundation (Grant No. 17-12-01134). The authors are grateful to Professor S. Preu and Dr. C. Marquardt for the help with experiment. We would like to thank Dr. U. Vogl, Dr. M. Chekhova, and K. Spasibko for fruitful discussions. Periodically poled lithium niobate samples were kindly provided by Dr. I. I. Naumova.

<sup>1</sup> D. N. Klyshko, *Photons and Nonlinear Optics* (Gordon and Breach Science, New York, 1988).

<sup>2</sup> G. Kh. Kitaeva and A. N. Penin, “Spontaneous parametric down-conversion,” *JETP Lett.* **82**(6), 350–355 (2005).

<sup>3</sup> D. N. Klyshko, “Utilization of vacuum fluctuations as an optical brightness standard,” *Sov. J. Quantum Electron.* **7**(5), 591–595 (1977).

<sup>4</sup> D. N. Klyshko, G. Kh. Kitaeva, and A. N. Penin, “Parametric photometer—A device for standardless non-destructing measurement of radiation spectral brightness,” *Proc. SPIE* **1869**, 250–257 (1993).

<sup>5</sup> A. Migdall, R. Datla, A. Sergienko, J. S. Orszak, and Y. H. Shih, “Measuring absolute infrared spectral radiance with correlated visible photons: Technique verification and measurement uncertainty,” *Appl. Opt.* **37**(16), 3455–3463 (1998).

<sup>6</sup> J. Hollandt, J. Seidel, R. Klein, G. Ulm, A. Migdall, and M. Ware, “Primary sources for use in radiometry,” in *Optical Radiometry*, Experimental Methods in the Physical Sciences, edited by A. C. Parr, R. U. Datla, and J. L. Gardner (Elsevier, Amsterdam, 2005), Vol. 41, Chap. 5, pp. 213–290, ISBN: 9780124759886.

<sup>7</sup> A. N. Penin and D. N. Klyshko, “Absolute measurements of radiation sources spectral brightness and detectors quantum efficiency,” *Proc. SPIE* **1562**, 143–148 (1991).

<sup>8</sup> D. N. Klyshko and A. N. Penin, “The prospects of quantum photometry,” *Sov. Phys.-Usp.* **30**(8), 716 (1987).



- <sup>9</sup> G. Kh. Kitaeva, P. V. Yakunin, V. V. Kornienko, and A. N. Penin, "Absolute brightness measurements in the terahertz frequency range using vacuum and thermal fluctuations as references," *Appl. Phys. B* **116**(4), 929–937 (2014).
- <sup>10</sup> G. Kh. Kitaeva, S. P. Kovalev, A. N. Penin, A. N. Tuchak, and P. V. Yakunin, "A method of calibration of terahertz wave brightness under nonlinear-optical detection," *J. Infrared, Millimeter, Terahertz Waves* **32**, 1144–1156 (2011).
- <sup>11</sup> G. Kh. Kitaeva, V. V. Tishkova, I. I. Naumova, A. N. Penin, C. H. Kang, and S. H. Tang, "Mapping of periodically poled crystals via spontaneous parametric down-conversion," *Appl. Phys. B* **81**(5), 645–650 (2005).
- <sup>12</sup> K. A. Kuznetsov, H. C. Guo, G. Kh. Kitaeva, A. A. Ezhov, D. A. Muzychenko, A. N. Penin, and S. H. Tang, "Characterization of periodically poled LiTaO<sub>3</sub> crystals by means of spontaneous parametric down-conversion," *Appl. Phys.* **83**(2), 273 (2006).
- <sup>13</sup> K. L. Vodopyanov, M. M. Fejer, X. Yu, J. S. Harris, Y.-S. Lee, W. C. Hurlbut, V. G. Kozlov, D. Bliss, and C. Lynch, "Terahertz-wave generation in quasi-phase-matched GaAs," *Appl. Phys. Lett.* **89**, 141119 (2006).
- <sup>14</sup> G. H. Ma, S. H. Tang, G. Kh. Kitaeva, and I. I. Naumova, "Terahertz generation in Czochralski-grown periodically poled Mg:Y:LiNbO<sub>3</sub> by optical rectification," *J. Opt. Soc. Am. B* **23**(1), 81–89 (2006).
- <sup>15</sup> T. D. Wang, S. T. Lin, Y. Y. Lin, A. C. Chiang, and Y. C. Huang, "Forward and backward terahertz-wave difference-frequency generations from periodically poled lithium niobate," *Opt. Express* **16**(9), 6471–6478 (2008).
- <sup>16</sup> D. A. Walsh, P. G. Browne, M. H. Dunn, and C. F. Rae, "Intracavity parametric generation of nanosecond terahertz radiation using quasi-phase-matching," *Opt. Express* **18**(3), 13951–13963 (2010).
- <sup>17</sup> G. Kh. Kitaeva, "Frequency conversion in aperiodic quasi-phase-matched structures," *Phys. Rev. A* **76**, 043841 (2007).
- <sup>18</sup> P. E. Schoen and D. A. Jackson, "The iodine filter in Raman and Brillouin spectroscopy," *J. Phys. E: Sci. Instrum.* **5**(6), 519–521 (1972).
- <sup>19</sup> H. Okajima and H. Hamaguchi, "Fast low frequency (down to 10 cm<sup>-1</sup>) multichannel Raman spectroscopy using an iodine vapor filter," *Appl. Spectrosc.* **63**(8), 958–960 (2009).
- <sup>20</sup> V. V. Kornienko, G. Kh. Kitaeva, I. I. Naumova, A. N. Tuchak, A. N. Penin, and P. V. Yakunin, "Evaluating the spectral sensitivity of the nonlinear-optical terahertz wave radiation detectors via spontaneous parametric down-conversion spectra," *Opt. Spectrosc.* **116**(4), 520–528 (2014).
- <sup>21</sup> K. A. Kuznetsov, G. Kh. Kitaeva, S. P. Kovalev, S. A. Germansky, A. M. Buryakov, A. N. Tuchak, and A. N. Penin, "Complex extraordinary dielectric function of Mg-doped lithium niobate crystals at terahertz frequencies," *Appl. Phys. B* **122**, 223 (2016).
- <sup>22</sup> G. K. Kitaeva, I. I. Naumova, A. A. Mikhailovsky, P. S. Losevsky, and A. N. Penin, "Visible and infrared dispersion of the refractive indices in periodically poled and single domain Nd:Mg:LiNbO<sub>3</sub> crystals," *Appl. Phys. B* **66**(2), 201–205 (1998).
- <sup>23</sup> M. Schall, H. Helm, and S. R. Keiding, "An infrared properties of electro-optic crystals measured by THz time-domain spectroscopy," *Int. J. Infrared Millimeter Waves* **20**(4), 595–604 (1999).
- <sup>24</sup> R. Le Bihan, D. Averty, D. Pain, A. L. Aleksandrovski, and I. I. Naumova, "Study of lithium niobate with periodically reversed domains," *Ferroelectrics* **172**(1), 181–186 (1995).
- <sup>25</sup> I. I. Naumova, "The growth of Y-doped, Dy-doped, Nd-doped, and Mg-doped single lithium niobate crystals with a regular domain-structure," *Crystallogr. Rep.* **39**(6), 1029 (1994).
- <sup>26</sup> I. I. Naumova, N. F. Evlanova, O. A. Gliko, and S. V. Lavrichev, "Czochralski-grown lithium niobate with regular domain structure," *Ferroelectrics* **190**(1), 107–112 (1997).
- <sup>27</sup> N. F. Evlanova, I. I. Naumova, T. O. Chaplina, S. A. Blokhin, and S. V. Lavrishchev, "Periodically poled Y:LiNbO<sub>3</sub> single crystal: Impurity distribution and domain wall location," *J. Cryst. Growth* **223**(1-2), 156–160 (2001).
- <sup>28</sup> I. I. Naumova, N. F. Evlanova, S. A. Blokhin, T. O. Chaplina, and A. A. Novikov, "Regular domain structure in a lithium niobate crystal—Period stabilization," *Crystallogr. Rep.* **48**(4), 705–706 (2003).
- <sup>29</sup> I. Shoji, T. Kondo, A. Kitamoto, M. Shirane, and R. Ito, "Absolute scale of second-order nonlinear-optical coefficients," *J. Opt. Soc. Am. B* **14**(9), 2268–2294 (1997).
- <sup>30</sup> A. Ridah, P. Bourson, M. D. Fontana, and G. Malovichko, "The composition dependence of the Raman spectrum and new assignment of the phonons in LiNbO<sub>3</sub>," *J. Phys.: Condens. Matter* **9**(44), 9687–9693 (1997).
- <sup>31</sup> M. C. Collodo, F. Sedlmeir, B. Sprenger, S. Svitlov, L. J. Wang, and H. G. Schwefel, "Sub-kHz lasing of a CaF<sub>2</sub> whispering gallery mode resonator stabilized fiber ring laser," *Opt. Express* **22**(16), 19277 (2014).